

Journal of Materials Chemistry A

Accepted Manuscript



This is an *Accepted Manuscript*, which has been through the Royal Society of Chemistry peer review process and has been accepted for publication.

Accepted Manuscripts are published online shortly after acceptance, before technical editing, formatting and proof reading. Using this free service, authors can make their results available to the community, in citable form, before we publish the edited article. We will replace this *Accepted Manuscript* with the edited and formatted *Advance Article* as soon as it is available.

You can find more information about *Accepted Manuscripts* in the [Information for Authors](#).

Please note that technical editing may introduce minor changes to the text and/or graphics, which may alter content. The journal's standard [Terms & Conditions](#) and the [Ethical guidelines](#) still apply. In no event shall the Royal Society of Chemistry be held responsible for any errors or omissions in this *Accepted Manuscript* or any consequences arising from the use of any information it contains.

ARTICLE

Composite films as high performance anode materials in thin film lithium-ion batteries

Cite this: DOI: 10.1039/x0xx00000x

Jie Lin, Jianlai Guo, Chang Liu, Hang Guo*

Received 00th January 2012,
Accepted 00th January 2012

DOI: 10.1039/x0xx00000x

www.rsc.org/

In order to utilize silicon (Si) as anode material for thin film lithium-ion batteries, the magnetron sputtering technology is used to deposit copper doped tin oxide (SnCu_xO_y) and lithium phosphorous oxynitride (LiPON) on Si substrates to obtain composite films. The material characterizations indicate that the $\text{SnCu}_x\text{O}_y/\text{LiPON}$ film is homogeneously deposited with nanoscale pores and particles, and it can activate Si substrate largely, alleviate the volumetric expansion effectively and facilitate an excellent electrochemical performance. This paper provides guidance to achieve activity and stability in developing high performance Si anode materials for advanced secondary batteries.

Introduction

With the rapid development of Micro Electro Mechanical System (MEMS) and microelectronic technologies in military, medicine, aerospace and other fields, searching suitable micro power devices for supplying energy to micro/nano devices and systems is of great importance for realizing miniaturization and integration of a whole system.¹ Thin film lithium-ion batteries (LIBs)² are talent showing themselves as micro power sources for the flexible size, safety, high energy density and ability to be integrated on one chip. However, the most critical drawback of lithium metal as anode³ is the extremely active chemical property, and the commonly used graphite has a low capacity,⁴ both of which significantly affect and limit the wide application of thin film LIBs. As a result, lithium free anode materials (such as Sn, Si and Ge) with high capacities attract wide attentions,⁵ but further research is still required to address the severe volumetric expansion/contraction during lithiation/delithiation. Many improved methods are reported to settle the problem, e.g. doping metal,⁶ synthesizing composite,⁷ designing microstructure⁸ or nanostructure⁹ and using structural/physical buffer.¹⁰ Nevertheless, to the best of our knowledge, almost all anode materials are deposited or synthesized on copper,¹¹ nickel,¹² titanium¹³ or gold-coated silicon.¹⁴ Few works consider using a lithium-ion (Li^+) conductive film as the key layer to activate Si substrate and fabricate high performance composite films. Thus, the volumetric change may be greatly reduced and composite films can be used to store Li^+ . Generally, Si based materials serve as the substrates for microelectronic and MEMS devices. Therefore, the Si bulk materials combined with Li^+ conductive films as high performance anodes are extremely attractive for thin film LIBs.

Since SnO_x is first suggested as anode material for LIBs,¹⁵ many groups begin to research SnO_x as anode electrode.¹⁶ It is believed that SnO_x is irreversibly reduced to Sn in the initial discharge,¹⁷ and further researches prove that the reaction mechanism in SnO_x is by alloying and de-alloying.¹⁸ Tin based thin films deposited by using magnetron sputtering are uniform and easily doped with other metals (Cu, Ag, Fe, etc.), exhibiting a high capacity and good cycle performance.¹⁹ On the other hand, lithium phosphorous oxynitride

(LiPON) generally obtained by sputtering Li_3PO_4 in a N_2 atmosphere is widely used as solid state electrolyte²⁰⁻²², can transport Li^+ and has a wide electrochemical window (> 5.5 V). Besides, LiPON has been used as a protective film for LiCoO_2 , LiMn_2O_4 , Li-Mn-Ni-O , etc.²³⁻²⁵ However, no one makes full use of porous LiPON as a transition layer to activate and protect Si. Si materials, especially particles,²⁶ powders²⁷ or polycrystals²⁸, are extensively studied as anodes and reported to have a low discharge potential of less than 0.5 V with an ultrahigh theoretical capacity of 4200 mAh g^{-1} . But Si has few practical applications for LIBs due to its big volumetric expansion up to 420% during the repeated Li^+ insertion and extraction.²⁹

In our study, we turn to a new idea that is to utilize composite thin films as anode materials, i.e. combination of copper doped tin oxide (SnCu_xO_y), LiPON and Si, expecting that they can possess reliable properties, such as a high capacity, good cycle performance and acceptable conductivity. In this work, various samples of SnO_x , SnCu_xO_y , $\text{SnCu}_x\text{O}_y/\text{Si}$ and $\text{SnCu}_x\text{O}_y/\text{LiPON}/\text{Si}$ (excluding the current collector) are fabricated by magnetron sputtering and compared as anode materials for thin film LIBs. The results show that the $\text{SnCu}_x\text{O}_y/\text{LiPON}/\text{Si}$ film exhibits the highest capacity ($441 \mu\text{Ah cm}^{-2}$ after 100 cycles) and the best cycle performance. Furthermore, a porous composite film $\text{SnCu}_x\text{O}_y/\text{LiPON}$ is obtained and the slaking structure is found favourable for alleviating volumetric change.^{32, 33} This study indicates that the composite films can significantly optimize the transition interface, protect Si anodes and act as high performance anode materials for thin film LIBs.

Experimental section

1 Fabrication of nanocomposite films

All films were fabricated by using radio frequency (RF) magnetron sputtering technology (JC500-3/D magnetron sputtering system). In this study, N-type 4-in (100) Si wafers were used and the thickness was $500 \mu\text{m}$. The fabrication process is schematically illustrated in Fig. 1. After the standard cleaning and surface activation, Ti/Au with a thickness of 20/200 nm were consecutively sputtered on the Si substrates. Here Ti was used as the coherent layer and Au as the

current collector for LIBs. Afterwards, a LiPON film (~ 100 nm) was deposited on the other side of the Si substrates with a 6-in Li_3PO_4 target (purity, 99.99%) in a N_2 atmosphere. During the process, the chamber pressure was kept at 1.3 Pa and the sputtering power was 100 W. Then a SnCu_xO_y film (~ 200 nm) was deposited by using co-sputtering technology, where three pieces of copper were put on a 6-in Sn target (purity, 99.99%). The chamber pressure was kept at 1.33 Pa with an Ar: O_2 ratio of 1: 2 and the sputtering power was 120 W.

In the end, a composite film of $\text{SnCu}_x\text{O}_y/\text{LiPON}/\text{Si}/\text{Collector}$ was obtained and defined as sample A. Here, the ‘‘Collector’’ represents the Ti/Au films. In order to make comparisons, sample B, C and D were also fabricated as shown in Fig. 1. In sample B, SnCu_xO_y was sputtered on Au layer, and described as $\text{SnCu}_x\text{O}_y/\text{Collector}/\text{Si}$. In sample C, SnCu_xO_y was sputtered on Si as $\text{SnCu}_x\text{O}_y/\text{Si}/\text{Collector}$. In sample D, SnO_x was sputtered on Au layer as $\text{SnO}_x/\text{Collector}/\text{Si}$.

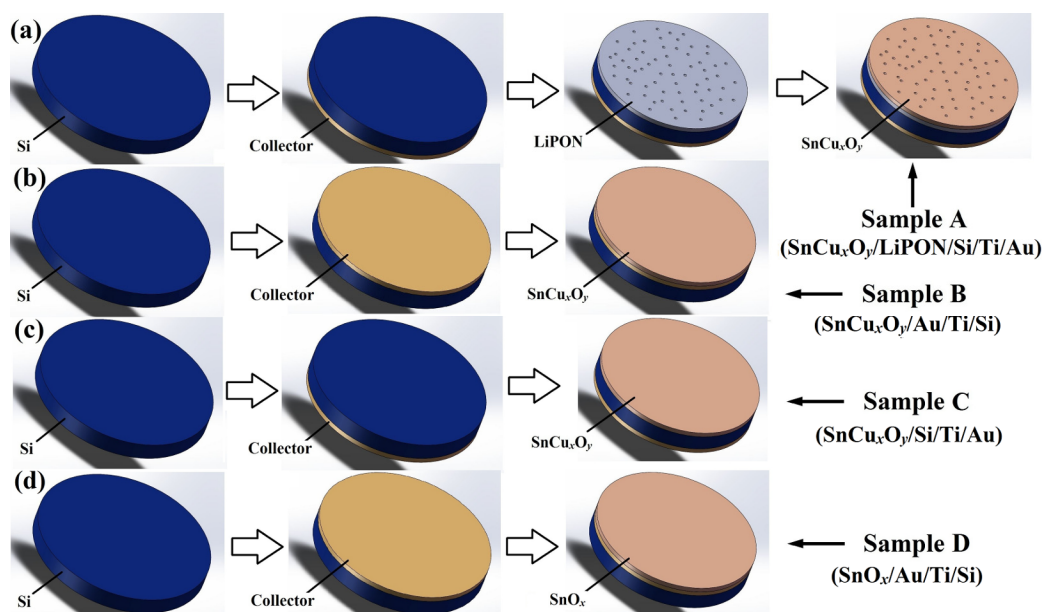


Fig. 1 (a, b, c) Fabrication process and structures of sample A, B, C and D.

2 Material characterizations

Small pieces in a same size of $10\text{ mm} \times 10\text{ mm}$ were cut from the prepared samples. The X-ray diffraction (XRD) equipment (Rigaku Ultima IV) with $\text{Cu K}\alpha$ radiation was used to identify the crystal structures. The morphology and composition of the samples were investigated using a ZEISS Sigma scanning electron microscope (SEM) equipped with an energy dispersive X-ray spectrum (EDS) analyzer. Also, the morphology was testified using a Nanoscope IIIa multimode atomic force microscope (AFM), and the chemical composition was checked by X-ray photoelectron spectroscopy (XPS) on a PHI Quantum 2000 Scanning ESCA Microprobe.

3 Electrochemical measurements

The electrochemical properties of composite films were measured in coin cells (CR2016) assembled in an Ar-filled glove box. The above composite film samples were chosen as the working electrodes, Li metal foils as the counter electrodes, a polypropylene (PP) film (Celgard 2400) as the separator, and 1.0 mol/L LiPF_6 mixed with ethylene carbonate, dimethyl carbonate and diethyl carbonate (EC/DMC/DEC, 1:1:1 in volume) as the electrolyte. After the coin cells were shelved for ~ 12 h, the galvanostatic charge/discharge tests were conducted on Neware BTS5V/1mA battery test systems (Shenzhen, China). The cyclic voltammetry (CV) tests were performed on Arbin-BT2000 test instruments at a scan rate of 0.5 mV s^{-1} between 0 and 3.0 V. It was noted that all tests were carried out at room temperature.

Results and discussion

1 Morphology and structural properties

The surface morphology of sample A (Fig. 2a) demonstrates an obviously porous surface coated with nanoscale particles. The porous film is expected to release the volumetric expansion during charge/discharge and increase the specific surface area for reactions. As the microstructure of LiPON is gross³⁴ and it is easy to form pores after exposing to oxygen or moisture,³⁵ an increased porosity is generated during sputtering SnCu_xO_y in an oxygen atmosphere. As expected, similar structures can not be observed on the surface of sample B (Fig. 2b), and the nanoscale grains nucleate on the overall substrate in close contact. The cross section SEM image of sample A is presented in Fig. 2c. Color change of layers can be observed from SnCu_xO_y to LiPON. The thickness of SnCu_xO_y and LiPON is measured to be ~ 200 and ~ 100 nm. A gold-coated Si substrate is used to improve the conductivity during observing, and some pores of LiPON can be seen as redacted in Fig. 2c. Thus the SnCu_xO_y film sputtered subsequently is porous as well with a rough appearance. The interfaces between the layers of sample B (Fig. 2d) are smooth without any defects such as pinholes or cracks. It can be predicted that the stacked layers may lead to severe stress rupture after cycling for a long time, and the ingenious using of porous LiPON film may promote a better cycle performance for sample A.

The elementary composition of sample A and B is analyzed by EDS characterization (Fig. 2e and f) from Fig. 2a and b. Silicon element in the abundant substrate is neglected in the spectrums. The presence of Oxygen, Phosphorus, Nitrogen, Copper and Tin evidences the successful deposition of SnCu_xO_y and LiPON in sample A. Especially, the ratio of Copper to Tin content in sample A (1.14: 1) is almost the same as that in sample B (1.14: 1), which confirms that films are homogeneously deposited on all substrates.

The 3D AFM images of sample A and B are shown in Fig. 2g. In sample A, the additional LiPON film leads to an increased surface roughness, and the maximum height gap is 95.1 nm. As mentioned before, the sputtered LiPON film (~100 nm) is porous and the subsequent growth barely occurs on the previously formed pores, producing a porous SnCu_xO_y film as well. While in sample B, the morphology is relatively flat with a biggest fall of 9.3 nm, in keeping with SEM images.

The postmortem morphologies of sample A before cycling and after 100 cycles are depicted in Fig. 2h. Before cycling, the surface is smooth without any defects in a relatively large scale. After 100 cycles, the structure of Si substrate is intact and no obvious fragmentation can be seen under the same scale. This stems from the buffering effect and prevented direct contact between Si and electrolyte by the SnCu_xO_y/LiPON film. The results indicate that the volumetric change of sample A is eased effectively.

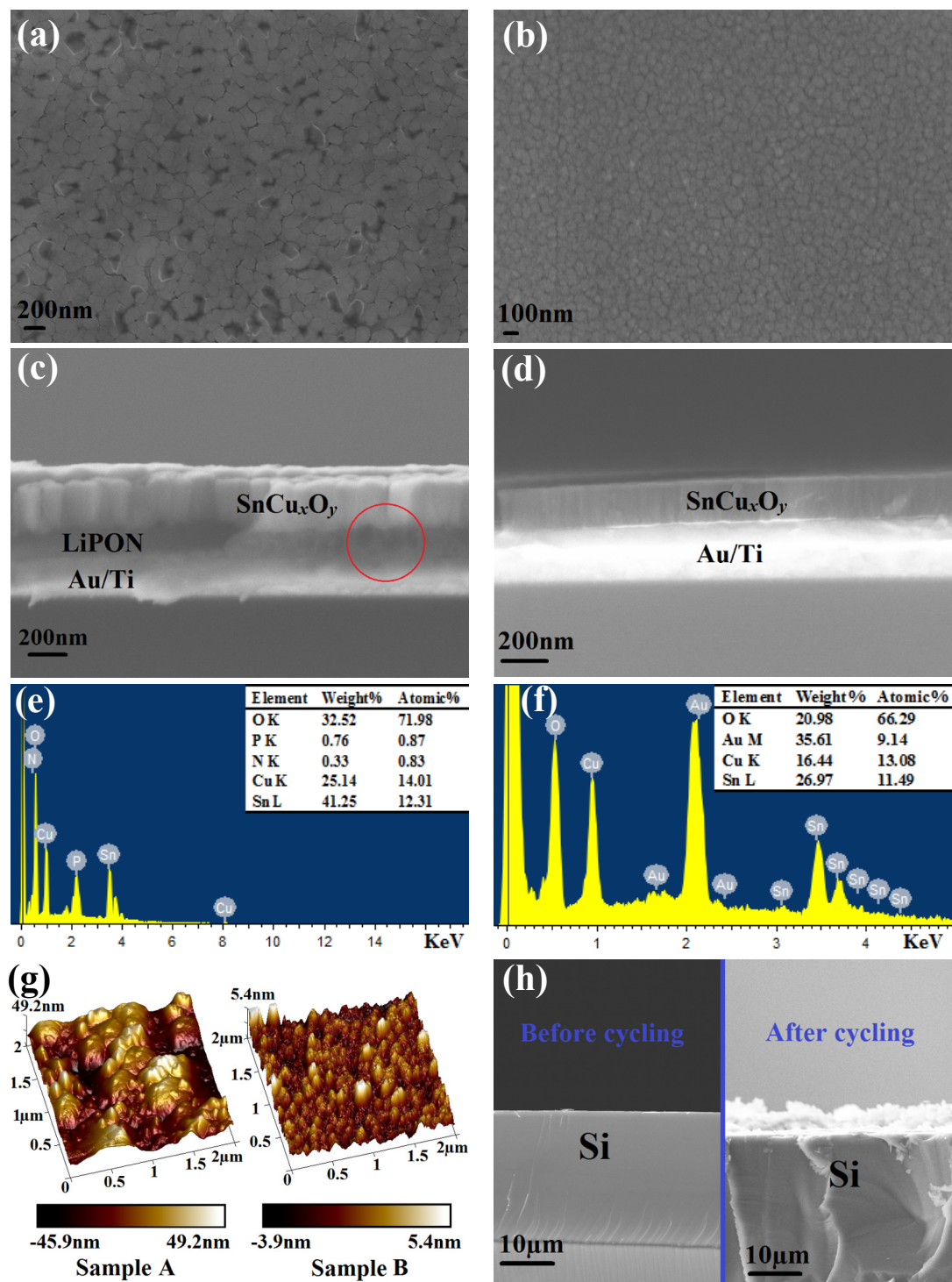


Fig. 2 (a, b) Surface SEM images of sample A and B, (c, d) cross section SEM images of sample A and B, (e, f) EDS patterns of sample A and B from (a, b), (g) 3D AFM images of sample A and B, and (h) cross section SEM images of sample A before cycling and after 100 cycles.

The XRD patterns of different films are presented in Fig. 3a. In view that oxygen may be absorbed by LiPON to form pores³⁵ during sputtering SnCu_xO_y , the lack oxygen content on the surface of sample A will induce more SnO to nucleate than sample B.³⁶ In general, the LiPON film tends to be amorphous.²¹ So apart from the peak of substrate, only reduced peaks of SnO can be indexed in sample A, while weakened peaks of SnO_2 and Au can be seen in sample B. In terms of pure SnO_x or Cu film prepared at the same experimental conditions, intense peaks of SnO_2 or Cu can be observed, but they are not fit with the patterns of sample A or B. In a word, the doping coppers and LiPON film lead SnO_x film to be amorphous as reported.¹⁵

The elements in the surface layer of sample A is confirmed by XPS analysis (Fig. 3b) and no fitting is applied. The tin 3d peaks located at 486.6 and 495.1 eV with a peak splitting of 8.5 eV

indicating SnO or SnO_2 , because the discrimination between SnO and SnO_2 is only a very small shift in the binding energy. The copper 2p peaks located at 932.4 and 952.2 eV with a peak separation of 19.8 eV indicating Cu or Cu_2O . But according to Auger spectrum (copper lmm), the main Auger peak at 570.1 eV corresponds to Cu^+ .³⁷ The oxygen 1s peak at 530.5 eV is associated with oxides. The formula obtained is $\text{Sn}_{0.29}\text{Cu}_{0.25}\text{O}_{0.46}$, consistent with the results that the composite film is composed of Cu_2O , SnO and SnO_2 . Since only the surface layer can be detected by XPS, and the oxygen inside LiPON contributes largely to the ratio, the oxygen content of XPS is less than the result of EDS. Consequently, the films are all successfully deposited on Si substrates combining the SEM, EDS, XRD and XPS analysis.

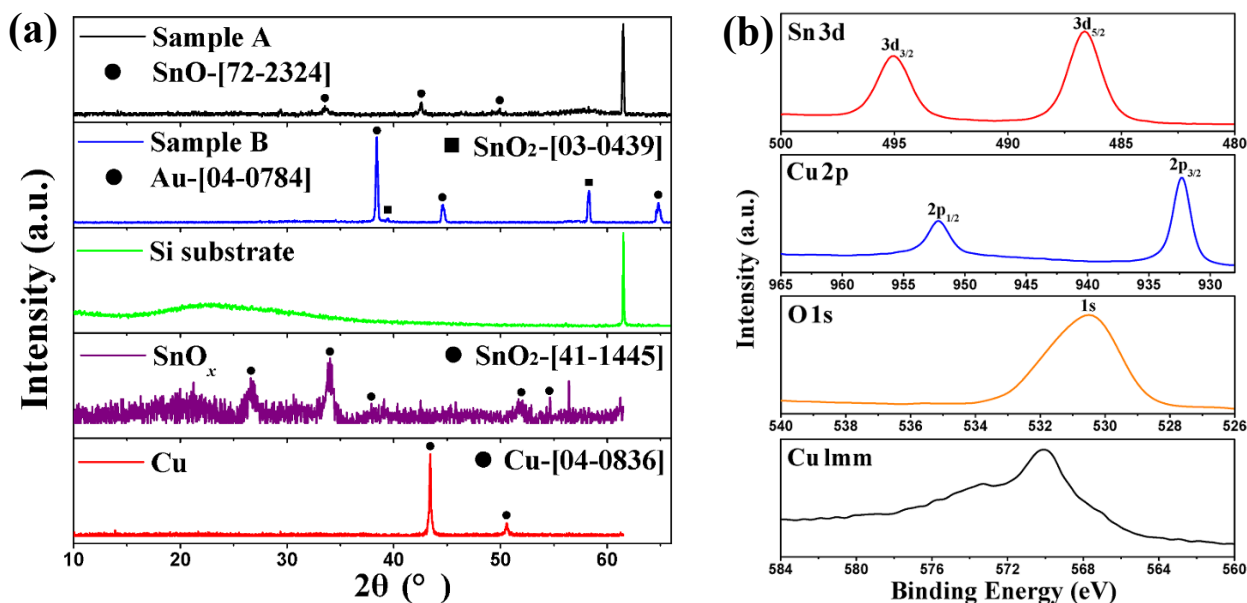


Fig. 3 (a) XRD patterns of sample A, B, Si, SnO_x and Cu films. (b) XPS spectra of surface layer in sample A.

2 Galvanostatic charge/discharge curves

The Au film is a blocking electrode that Li^+ can not easily pass through and insert into Si, but LiPON film can deliver Li^+ and the liquid electrolyte may permeate into pores to react with Si. As a result, the main effective materials of sample A, B, C and D are SnCu_xO_y -Si (combined by LiPON), SnCu_xO_y , SnCu_xO_y -Si and SnO_x , respectively. The voltage range during charge/discharge for sample A and C is 0.12-1.2 V, and 0.1-1.2 V for sample B and D. It is found when the cut-off voltage is below 0.1 V, the electrode will experience mechanical fractures resulting in the collapse of Si materials.³⁸ So, in order to achieve a compromise between capacity and cycle performance, a narrower voltage window is employed and thus just the surface of Si wafer participates in the lithiation process. The current density for all samples used to activate the electrodes in the initial two cycles is $20 \mu\text{A cm}^{-2}$ and then $40 \mu\text{A cm}^{-2}$ in the following cycles.

The charge/discharge curves of sample A are shown in Fig. 4a. The curves are similar to those of multilayer films, such as Sn,³⁹ Cu-Sn,⁴⁰ and Zn-Sn⁷, resulting from the gradually activation for each layer. The initial charge and discharge capacities are 298 and $403 \mu\text{Ah cm}^{-2}$ with an irreversible capacity loss of 26.05%. In the first cycle, a long discharge plateau at ~ 0.12 V can be seen and then disappears in the following cycles. This is associated with the

insertion of Li^+ into the Si material to form Li_xSi alloys,^{28, 31} and due to the activation for Si substrate through LiPON film. The initial charge plateaus at 0.25 and 0.5 V correspond to the Li^+ extraction from Li-Si and Li-Sn alloys.^{28, 30, 31} In the 5th cycle, the charge and discharge capacities are 187 and $188 \mu\text{Ah cm}^{-2}$ with a coulombic efficiency of nearly 100%. The results manifest the good reversible performance of sample A. The discharge plateaus range from 0.1 to 0.3 V, mainly attributed to the Li^+ storage process of Li-Sn alloys.^{13, 40} Whereas, the charge plateau at 0.25 V disappears, and only one slope plateau at ~ 0.5 V can be seen corresponding to the Li^+ extraction of Li-Sn alloys. In the 100th cycle, the charge/discharge capacities are 436 and $441 \mu\text{Ah cm}^{-2}$. The plateaus gradually elongate and become slopes, implying the transition of lithiation process from Sn to Si. On the other hand, the capacity is higher than that in the initial cycle, demonstrating the further activation of Si from substrate.

The charge/discharge curves of sample B are shown in Fig. 4b. The initial charge/discharge capacities are 63 and $208 \mu\text{Ah cm}^{-2}$ with an irreversible capacity loss of 72.59%. The irreversible discharge plateau at ~ 1.8 V is related to the reduction of SnO_2 ⁴¹ and the formation of solid electrolyte interphase (SEI) film.⁴² The subsequent plateau at ~ 0.5 V could be assigned to the irreversible transformation of Cu^+ to Cu. The characteristics agree well with XRD and XPS that SnO_2 and Cu^+ are combined into sample B. The

voltage profiles between 0.1-0.5 V are concerned with the reaction of Li-Sn alloys.⁴³ The discharge curves in the following cycles associated with the alloying of Li-Sn are steep, which are similar to the 5th discharge curve of sample A. The initial charge plateaus at 0.3-0.6 V is related to the dealloying of Li-Sn. The charge curves do not change obviously with the increase in cycle numbers.

The charge/discharge curves of sample C (Fig. 4c) are almost the same as sample B except the initial broad plateau, which may be affected by the irreversible synergetic lithiation of Sn and Si. Without LiPON film, the Si substrate can not be activated and the effective material is only SnCu_xO_y, indeed. The mechanism can be attributed to the raised lithiation potential by the additional Li⁺ of LiPON⁴⁴ and the prevented dissolution of effective material by the protective films.⁴⁵

The charge/discharge curves of sample D (Fig. 4d) are in accord with the voltage profiles of pure SnO_x.³⁰ Compared with SnCu_xO_y (Fig. 4b), the voltage profile at ~0.5 V related to Cu⁺ is absent and the voltage plateaus (~0.2 and 0.4 V during discharge and charge, respectively) are more apparent. The distinction can be ascribed to the abundant crystal SnO₂ in sample D as shown in XRD.¹⁶

In comparison, the capacity ranking after 100 cycles is sample A, B, D and C. Furthermore, the Si substrate of sample C can not be activated effectively without LiPON film. As a result, the SnCu_xO_y/LiPON/Si/Collector composite exhibits the significantly highest capacity.

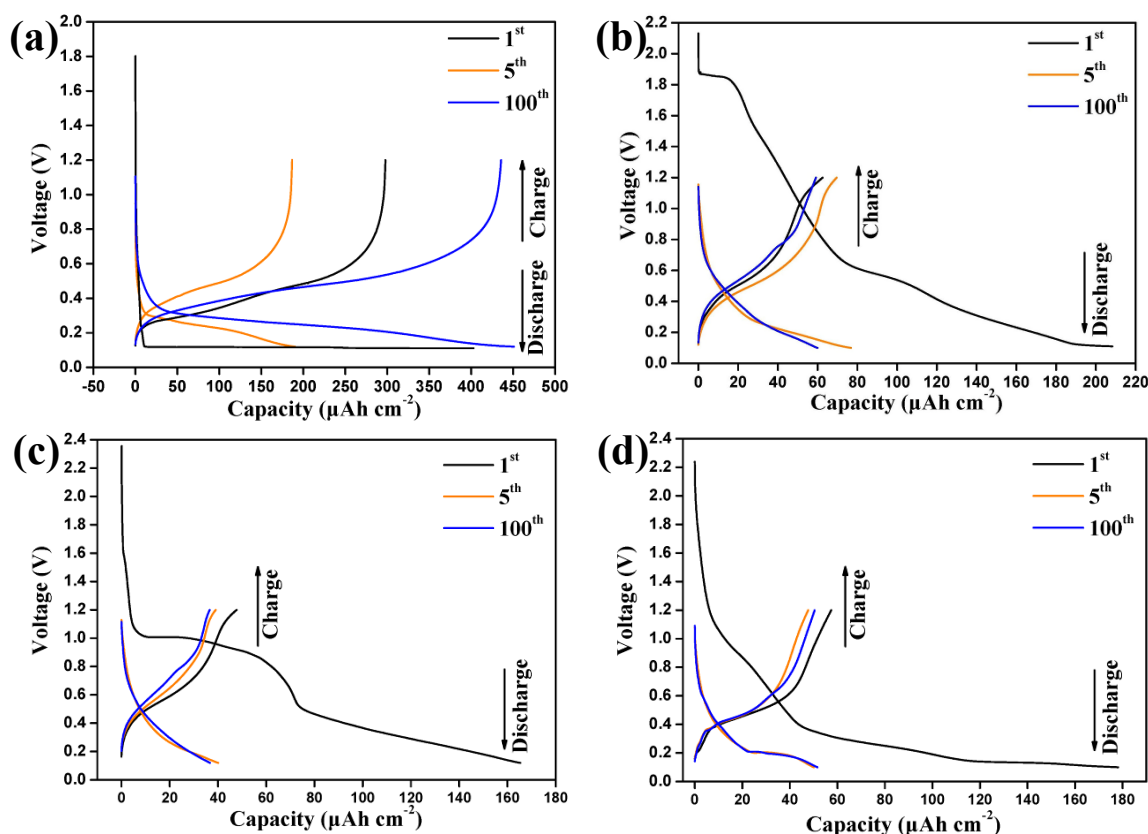
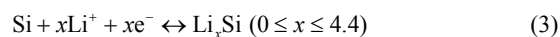
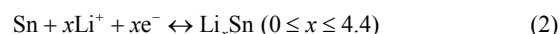


Fig. 4 (a, b, c, d) Galvanostatic charge/discharge curves of sample A, B, C and D.

3 Cycle performances

The cycle performances of all samples are shown in Fig. 5a. Among them, Sample A exhibits the highest capacity and a gradually increasing capacity as the Li⁺ diffusion kinetics inside the Si substrate are developed by an activation of low density current. The phenomenon can be found in SnO_x¹⁴ and Sn-Cu alloys⁴⁰ as reported, but only focus on the first several cycles as sample B. The effective material of sample B is SnCu_xO_y, and the structure is mechanically stable as shown in SEM images. In addition, the doped coppers not only can improve the electronic conductivity⁴⁶ but also ease the volumetric expansion as a conductive matrix.⁴⁷ Thus the mass capacity of sample B is ~1000 mAh g⁻¹ in the first several cycles and then slowly fades, which is superior to reported Cu-Sn thin film,⁴⁸ sample C and D. Sample C is fabricated by sputtering SnCu_xO_y film on Si substrate. The conductivity of Si/Collector in sample C is less than that of Collector/Si in sample

B and D. As a consequence, the last reversible capacity is only ~500 mAh g⁻¹, but comparable to the reported results.¹⁹



The cycle curve of sample A can be divided into three sections: the first four cycles with a decreasing capacity, the 5th to 50th cycles with a stable capacity and the 51st to 100th cycles with an increasing capacity. The drop in the first section is caused by some irreversible reactions including Eq. (1). A series of lithiation reactions including the alloying and dealloying of Sn, Li-Sn and Li-Si alloys as Eq. (2) and (3) occur in the second section. The capacity of sample A keeps increasing in the last section due to the further activation of Si substrate and the domination of Eq. (3).

It is illustrated that sample A has an excellent capacity and cycle performance. This result can be understandably attributed to the following reasons: (I) Si act as not only a substrate but also an anode material after the activation. (II) $\text{SnCu}_x\text{O}_y/\text{LiPON}$ serves as the protective film to prevent the direct contact between Si and electrolyte. (III) The porous LiPON film provides enough space to release the volumetric expansion. (IV) SnCu_xO_y improves the capacity and conductivity of the composite films.

The first three cycles of CV curves of sample A are denoted in Fig. 5b. An obvious reduction peak at ~ 0.1 V with a large current is resulted from the alloying of Li-Si alloys⁴⁹ as Fig. 4a. In addition,

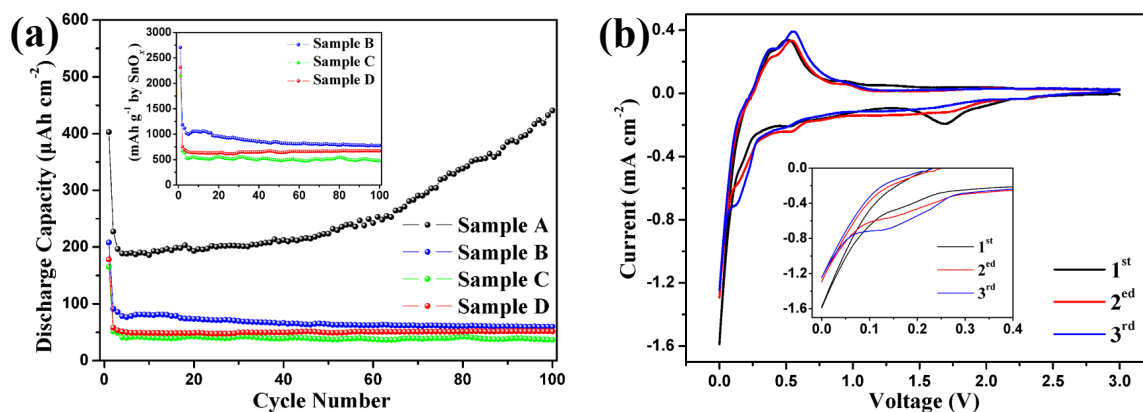


Fig. 5 (a) Cycle performance of all samples at a current density of $40 \mu\text{A cm}^{-2}$. Inset is capacities of sample B, C and D by the mass of SnO_x . (b) Initial three cycles of CV curves of sample A. Inset is detailed CV curves between 0-0.4 V.

Conclusions

Composite films are fabricated and studied as anode materials for thin film LIBs. Among the developed SnO_x , SnCu_xO_y , $\text{SnCu}_x\text{O}_y/\text{Si}$ and $\text{SnCu}_x\text{O}_y/\text{LiPON}/\text{Si}$ composite films (excluding the Collector), it is found that the $\text{SnCu}_x\text{O}_y/\text{LiPON}/\text{Si}$ film exhibits the best properties for the additional Li^+ supplied by LiPON, prevented dissolution of effective materials by the protective layer and released volumetric change by the porous microstructure. The capacity of sample A is $441 \mu\text{Ah cm}^{-2}$ even after 100 cycles, and the capacities of sample B, C and D are also comparable to the reported results. The method presented in this paper for activating Si can be applied to other potential materials and is useful for developing high performance thin film LIBs.

Acknowledgements

This work is financially supported by the Aviation Science Foundation of China (2008ZH68002), the New Century Talent Support Plan of the Ministry of Education of China (2007NCET-07-0723) and the National Natural Science Foundation of China (60936003).

Notes and references

Pen-Tung Sah Micro-Nano Science and Technology Institute, Xiamen University, Xiamen, Fujian, China. Email: hangguo@xmu.edu.cn.

1. L. C. Chia and B. Feng, *J Power Sources*, 2007, **165**, 455-480.
2. J. F. Whitacre, W. C. West and B. V. Ratnakumar, *J Electrochem Soc*, 2003, **150**, A1676.
3. B. J. Neudecker, N. J. Dudney and J. B. Bates, *J Electrochem Soc*, 2000, **147**, 517-523.

the reduction peak gradually decreases and moves to ~ 0.2 V with the cycles going on (the inset of Fig. 5b). This finding can be ascribed to the transition of lithiation process from Li-Si to Li-Sn in the first several cycles, in accord with the results of discharge curves. The two oxidation peaks at 0.37 and 0.55 V correspond to the Li^+ extraction from Li-Si alloys.⁵⁰ It is worth nothing that a distinct reduction peak at ~ 1.7 V in the initial cycle disappears in the following cycles. It is caused by the irreversible reaction (1) as well as the formation of SEI film. The redox peaks of sample A are identified with the charge/discharge plateaus.

4. R. Mukherjee, A. V. Thomas, A. Krishnamurthy and N. Koratkar, *Acs Nano*, 2012, **6**, 7867-7878.
5. S. Goriparti, E. Miele, F. De Angelis, E. Di Fabrizio, R. Proietti Zaccaria and C. Capiglia, *J Power Sources*, 2014, **257**, 421-443.
6. P. Ouyang, H. Zhang, Y. Wang, W. Chen and Z. Li, *Electrochim Acta*, 2014, **130**, 232-238.
7. L. Wang, S. Kitamura, K. Obata, S. Tanase and T. Sakai, *J Power Sources*, 2005, **141**, 286-292.
8. L. Ding, S. He, S. Miao, M. R. Jorgensen, S. Leubner, C. Yan, S. G. Hickey, A. Eychmuller, J. Xu and O. G. Schmidt, *Sci Rep*, 2014, **4**, 4647.
9. H. Zhang, Q. He, F. Wei, Y. Tan, Y. Jiang, G. Zheng, G. Ding and Z. Jiao, *Mater Lett*, 2014, **120**, 200-203.
10. Z. Wen, S. Cui, H. Kim, S. Mao, K. Yu, G. Lu, H. Pu, O. Mao and J. Chen, *J Mater Chem*, 2012, **22**, 3300.
11. X. Y. Fan, F. S. Ke, G. Z. Wei, L. Huang and S. G. Sun, *J Solid State Electr*, 2009, **13**, 1849-1858.
12. H. Liu, H. M. Cho, Y. S. Meng and Q. Li, *ACS Appl Mater Interfaces*, 2014, **6**, 9842-9849.
13. G. F. Ortiz, M. C. López, R. Alcántara and J. L. Tirado, *J Alloy Compd*, 2014, **585**, 331-336.
14. Y. L. Zhang, Y. Liu and M. L. Liu, *Chem Mater*, 2006, **18**, 4643-4646.
15. Y. Idota, *Science*, 1997, **276**, 1395-1397.
16. X. W. Guo, X. P. Fang, Y. Sun, L. Y. Shen, Z. X. Wang and L. Q. Chen, *J Power Sources*, 2013, **226**, 75-81.
17. W. F. Liu, X. J. Huang, Z. X. Wang, H. Li and L. Q. Chen, *J Electrochem Soc*, 1998, **145**, 59-62.

18. I. A. Courtney and J. R. Dahn, *J Electrochem Soc*, 1997, **144**, 2045-2052.
19. C. H. Wu, F. Y. Hung, T. S. Lui and L. H. Chen, *Mater Trans*, 2009, **50**, 381-387.
20. S.-H. Lee, P. Liu and C. E. Tracy, *Electrochemical and Solid-State Letters*, 2003, **6**, A275.
21. C. S. Nimisha, K. Y. Rao, G. Venkatesh, G. M. Rao and N. Munichandraiah, *Thin Solid Films*, 2011, **519**, 3401-3406.
22. F. Xu, N. J. Dudney, G. M. Veith, Y. Kim, C. Erdonmez, W. Lai and Y.-M. Chiang, *J Mater Res*, 2011, **25**, 1507-1515.
23. K.-H. Choi, J.-H. Jeon, H.-K. Park and S.-M. Lee, *J Power Sources*, 2010, **195**, 8317-8321.
24. N. J. Dudney, *J Power Sources*, 2000, **89**, 176-179.
25. L. Baggetto, R. R. Unocic, N. J. Dudney and G. M. Veith, *J Power Sources*, 2012, **211**, 108-118.
26. G. Y. Zhao, L. Zhang, Y. F. Meng, N. Q. Zhang and K. N. Sun, *Mater Lett*, 2013, **96**, 170-173.
27. H. Li, X. J. Huang, L. Q. Chen, Z. G. Wu and Y. Liang, *Electrochem Solid St*, 1999, **2**, 547-549.
28. H. Guo, H. Zhao, C. Yin and W. Qiu, *Materials Science and Engineering: B*, 2006, **131**, 173-176.
29. P. Hovington, M. Dontigny, A. Guerfi, J. Trottier, M. Lagace, A. Mauger, C. M. Julien and K. Zaghib, *J Power Sources*, 2014, **248**, 457-464.
30. J. Song, M.-Z. Cai, Q.-F. Dong, M.-S. Zheng, Q.-H. Wu and S.-T. Wu, *Electrochim Acta*, 2009, **54**, 2748-2753.
31. C. Yue, Y. J. Yu, J. Yin, T. L. Wong, Y. S. Zang, J. Li and J. Y. Kang, *Journal of Materials Chemistry A*, 2013, **1**, 7896-7904.
32. X. J. Zhu, Z. P. Guo, P. Zhang, G. D. Du, R. Zeng, Z. X. Chen, S. Li and H. K. Liu, *J Mater Chem*, 2009, **19**, 8360-8365.
33. Y. T. Han, X. Wu, Y. L. Ma, L. H. Gong, F. Y. Qu and H. J. Fan, *Crystengcomm*, 2011, **13**, 3506-3510.
34. K. Chung, W. S. Kim and Y. K. Choi, *J Electroanal Chem*, 2004, **566**, 263-267.
35. C. S. Nimisha, G. M. Rao, N. Munichandraiah, G. Natarajan and D. C. Cameron, *Solid State Ionics*, 2011, **185**, 47-51.
36. R. Kohler, H. Besser, M. Hagen, J. Ye, C. Ziebert, S. Ulrich, J. Proell and W. Pfleging, *Microsyst Technol*, 2011, **17**, 225-232.
37. L. Martin, H. Martinez, D. Poinot, B. Pecquenard and F. Le Cras, *The Journal of Physical Chemistry C*, 2013, **117**, 4421-4430.
38. H. Li, Z. X. Wang, L. Q. Chen and X. J. Huang, *Adv Mater*, 2009, **21**, 4593-4607.
39. Z. Du, S. Zhang, T. Jiang and Z. Bai, *Electrochim Acta*, 2010, **55**, 3537-3541.
40. S. Wang, W. Zhao, Y. Wang, X. Liu and L. Li, *Electrochim Acta*, 2013, **109**, 46-51.
41. R. A. Huggins, *Solid State Ionics*, 1998, **113**, 57-67.
42. M. Wu, X. Li, Q. Zhou, H. Ming, J. Adkins and J. Zheng, *Electrochim Acta*, 2014, **123**, 144-150.
43. A. Sivashanmugam, T. P. Kumar, N. G. Renganathan, S. Gopukumar, M. Wohlfahrt-Mehrens and J. Garche, *J Power Sources*, 2005, **144**, 197-203.
44. J. C. Li, L. Baggetto, S. K. Martha, G. M. Veith, J. Nanda, C. D. Liang and N. J. Dudney, *Advanced Energy Materials*, 2013, **3**, 1275-1278.
45. S. K. Martha, J. Nanda, Y. Kim, R. R. Unocic, S. Pannala and N. J. Dudney, *Journal of Materials Chemistry A*, 2013, **1**, 5587-5595.
46. X. Liu, F. Z. Liu, Q. Sun, A. M. C. Ng, A. B. Djuricic, M. H. Xie, C. Z. Liao, K. M. Shih and Z. F. Deng, *ACS Appl Mater Inter*, 2014, **6**, 13478-13486.
47. J. Z. Wang, N. Du, H. Zhang, J. X. Yu and D. R. Yang, *J Phys Chem C*, 2011, **115**, 23620-23624.
48. D. B. Polat, J. Lu, A. Abouimrane, O. Keles and K. Amine, *ACS Appl Mater Inter*, 2014, **6**, 10877-10885.
49. A. Kohandehghan, K. Cui, M. Kupsta, E. Memarzadeh, P. Kalisvaart and D. Mitlin, *Journal of Materials Chemistry A*, 2014, **2**, 11261-11279.
50. D. S. Wang, Z. B. Yang and D. Y. He, *Mater Lett*, 2014, **128**, 163-166.